An Expanded Murray-Davies Model of Tone Reproduction in Halftone Imaging

J. S. Arney, P. G. Engeldrum,* and H. Zeng*
Center for Imaging Science, Rochester Institute of Technology
Rochester, New York 14623-0887

Abstract

An empirical model has been developed to describe tone reproduction in halftone imaging. The model is based on experimental measurements of the image microstructure of halftone gray scales produced by offset lithography, thermal transfer, ink jet, and silver halide photography. Both traditional and stochastic halftone patterns are described by the model. Like the Yule-Nielsen model, which contains an arbitrary constant called the "Yule *n* factor", the model developed in the current study is derived from the Murray-Davies equation. However, the current model contains two empirical parameters, *w* and *v*. The *w* factor relates to the optical spread function of the paper relative to the spatial frequency of the halftone dots. The *v* factor relates to the distribution of colorant within the dot. The Yule-Nielsen model describes only the relationship between the mean reflectance, *R*, of the halftone image and the dot area fraction, F_i. The current model describes *R* versus F_i and also some experimental data on the image microstructure. With the Yule-Nielsen model, estimates of the *n* factor are traditionally made by fitting the model to *R* versus F_i data. With the current model, estimates of *w* and *v* are chosen to fit the image microstructure data. The resulting values of *w* and *v* provide an excellent fit with the mean reflectance, *R*, versus F_i data.

Introduction

The first optical model of tone reproduction in the halftone process was the Murray-Davies equation, first published in 1936.[1] This model describes a linear relationship

$$R(F_i) = F_i R_i + (1 - F_i)R_p \qquad (1)$$

between the reflectance, *R*, of the halftone image and the fractional area, F_i, of the image that is covered by halftone dots. The constants R_i and *R* are the reflectance of the ink and the paper, respectively. This model was extended by Neugebauer[2] in 1937 to describe full-color halftones. However, variation from linearity is typically observed and is often modeled with a modification of the Murray-Davies equation called the Yule-Nielsen equation.[3]

$$R(F_i) = [F_i R_i^{1/n} + (1 - F_i)R_p^{1/n}]^n. \qquad (2)$$

The Yule-Nielsen equation has been found to model tone and color reproduction quite well in many halftone systems.[4,5] Again R_i and R_p are reflectance values of the ink and the paper. However, the Yule "*n* factor" does not relate uniquely to a single physical property of the system. Rather, it is an empirical constant that is selected to provide the best fit between measured values of *R* and F_i. Values of *n* that fit well with experimental data are typically found to fall in the range $1 \le n \le 2$.[6] However, an interesting property of the Yule-Nielsen equation is that as *n* approaches infinity, the numerically calculated relationship between image density, $D = -\log(R)$, and F_i becomes linear.[3] In other words, the Yule-Nielsen equation seems to become something like the Beer-Lambert law as *n* approaches infinity. Intuitively, this seems to suggest that the Yule-Nielsen equation, though empirically derived, may reflect some fundamental theoretical behavior of the ink and paper system. However, two observations suggest that the Yule-Nielsen expression, though a useful and close approximation to halftone behavior, is not fundamentally a correct theoretical expression.

Observation One

Experimentally it is well known that the nonlinearity of *R* versus F_i is a manifestation of optical scattering of light within the halftone image.[7-10] The "*n* factor" is reported to be a function of the spatial frequency of the halftone and of the various optical and spatial properties of the ink and paper system. However, whereas excellent theoretical work has been published to derive the Yule-Nielsen expression from first principles, the Yule-Nielsen equation is found to result only from special limiting assumptions.[11,12] It seems, therefore, that the Yule-Nielsen equation is not a general expression that can be derived from first principles but an approximation of the underlying theory.

Observation Two

The Murray-Davies equation is essentially an expression of the law of conservation of energy: photon energy in this case. Reflectance values are linearly related to photon flux from the surface of the image, and one would expect reflectance to add. The Yule-Nielsen equation sums reflectance, and thus photon flux, raised to a power. This expression seems contrary to the conservation of energy, and it seems unlikely that the nonlinearity of *R*-versus-F_i data is a manifestation of a failure in the additivity of light energy.

The thrust of the work described below has been to preserve the linear additivity of reflectance in the Murray-Davies model but to modify the model to account for non-linear *R*-versus-F_i behavior. This has been done by recognizing that R_i and R_p are not constants, as assumed in Eqs. 1 and 2, but are themselves functions of F_i.

Experimental Observations of R_i and R_p as Functions of F_i

Light that enters the paper between the dots may be scattered laterally and emerge under a dot. Also, light entering the dot may scatter and emerge from the paper between the dots. The result is that the value of R_i is higher than observed for the ink at $F_i = 1$, and the value of R_p is lower than observed for the paper at $F_i = 0$. The significance of these scattered photons is that the overall reflectance of the dots and paper between the dots is a function of the relative size of the dots. Thus R_i and R_p are not really constants, but are functions of F_i. We denote these functions as $R_i(F_i)$ and $R_p(F_i)$ to emphasize the difference between the constant values assumed in the Murray-Davies and Yule-Nielsen equations. Appendix B summarizes definitions of different types of reflectance used in this manuscript.

The $R_i(F_i)$ and $R_p(F_i)$ functions are easily observed experimentally. Figure 1 is a digital image micrograph of a 65-lpi halftone image generated by a desktop ink-jet printer. The dot coverage is 50% ($F_i = 0.5$), and a region of unprinted paper is also shown. This image was captured digitally, as described in Appendix A, and from the digital image a histogram showing the frequency distribution of reflectance values in the image was generated, as shown in Fig. 2. It is evident in this histogram that the reflectance of the unprinted region of the paper is significantly higher than the reflectance of the paper between the dots.

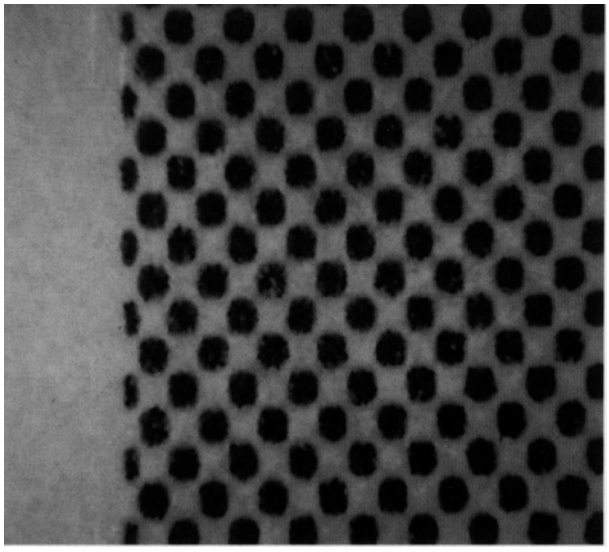

Figure 1. Micrograph of halftone pattern at approximately F_i = 0.5 from a 65-lpi ink-jet engine.

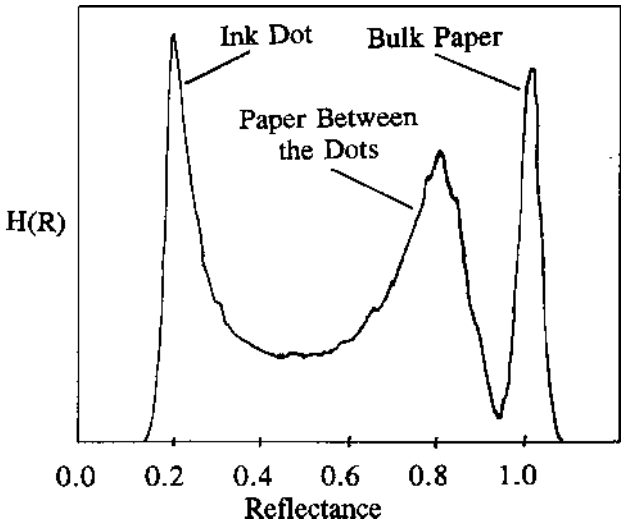

Figure 2. Histogram of reflectance values for the image shown in Fig. 1.

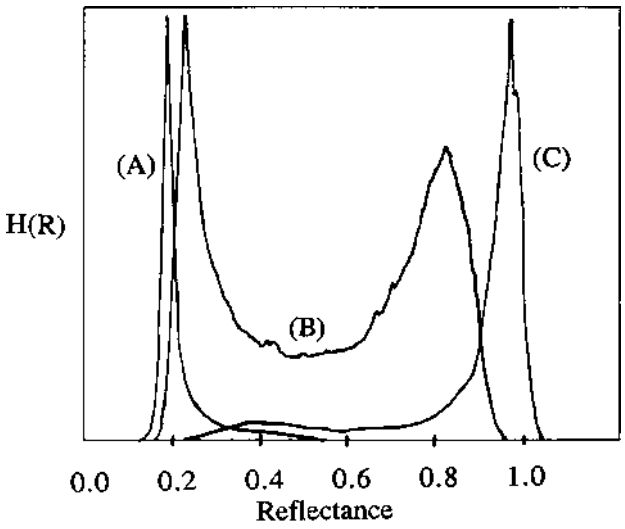

Figure 3. Reflectance histograms of ink-jet halftone gray scales at (A) $F_i = 0.05$, (B) $F_i = 0.5$, and (C) $F_i = 0.90$. Histogram frequencies, H(R), are normalized to unity for the highest peak.

The histograms shown in Fig. 3 were generated from digital images of the 65-lpi ink-jet gray scale, excluding the unprinted paper region. Data for different values of F_i, are shown and it is evident that as F_i increases, the height of the peak corresponding to the paper between the dots not only decreases, but also shifts to the left. Simultaneously, the height of the ink peak increases and shifts to the left. Mean values of R_i and R_p, taken to be the peaks in the histograms, were measured as functions of F_i. The data are summarized in Fig. 4. From Fig. 4, it seems qualitatively that the limiting value of R_p as F_i approaches zero is the same as R_i in the limit as F_i approaches 1. This makes sense if we consider the scattering of light within the paper in the halftone image. As illustrated in Fig. 5, the light emerging from the paper between the dots may have come from light incident on

the paper between the dots or from light incident on the dot and scattered into the paper between the dots. If the dot spacing is significantly larger than the average scattering distance, the latter photons can be ignored and the paper reflectance will be the same as the bulk reflectance of the paper, R_g. However, as F_i approaches unity, the majority of photons emerging from the paper are those that first passed through a dot. In this case, the limiting reflectance will be R_gT_i, where T_i is the transmittance of the ink layer. Similarly, it is evident that photons emerging from the dot in the limit as F_i approaches zero come predominantly from photons incident on the paper and scattered to emerge from the paper under the dot. Again the limiting reflection will be R_gT_i.

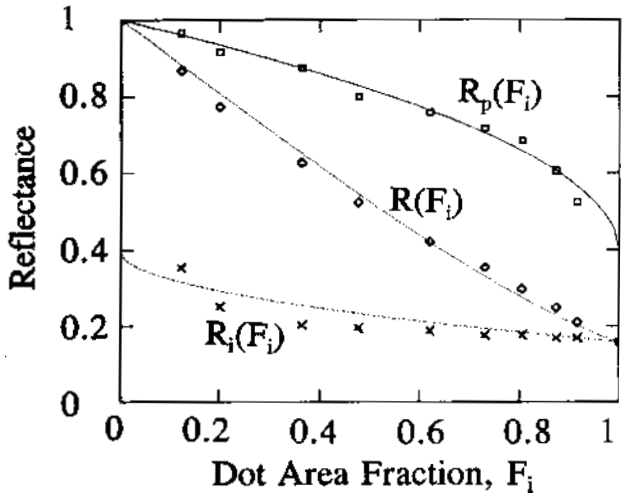

Figure 4. Ink-jet halftone data at 65-lpi. Reflectance versus dot area fraction, F_i, for overall reflectance, $R(F_i)$, ink reflectance, $R_i(F_i)$, and reflectance of paper between the dots $R_p(F_i)$. Solid lines are modeled with w = 0.526.

A Model That is Linear in Reflectance

At any given value of F_i, the macroscopic reflectance, R, that one measures with a traditional densitometer or spectrophotometer is an average reflectance over the field of view of the instrument. This field of view is typically large relative to the size of the halftone dots. The areas of the images captured to produce histogram data such as that in Fig. 3 were large relative to the dot size, so that the same mean reflectance can be calculated from the data in the histogram. Because the histogram is a probability density function, its integral from $r = 0$ to $r = 1$ is unity. Thus the average reflectance value in the image may be calculated from the histogram as follows.

$$R = \int_0^1 R \cdot H(R)\mathrm{d}R. \qquad (3)$$

We can integrate this function in two parts.

$$R = \int_0^{R_t} R \cdot H(R)\mathrm{d}R + \int_{R_t}^1 R \cdot H(R)\mathrm{d}R. \qquad (4)$$

The intermediate reflectance, R_t, is a threshold reflectance between dot and paper, as defined in Appendix A. Then if we approximate the values of R in the two integrals by the peak values, $R_i(F_i)$ and $R_p(F_i)$, from the histograms at each value of F_i, we have

$$R = R_i(F_i)\int_0^{R_t} H(R)\mathrm{d}R + R_p(F_i)\int_{R_t}^1 H(R)\mathrm{d}R. \qquad (5)$$

The two integrals in Eq. 5 are the fractions F_i and $F_p = 1 - F_i$. Thus we have the Murray-Davies equation,

$$R(F_i) = F_iR_i(F_i) + (1 - F_i)R_p(F_i), \qquad (6)$$

in which the functions, $R_i(F_i)$ and $R_p(F_i)$ have replaced the constants for paper and ink reflectance.

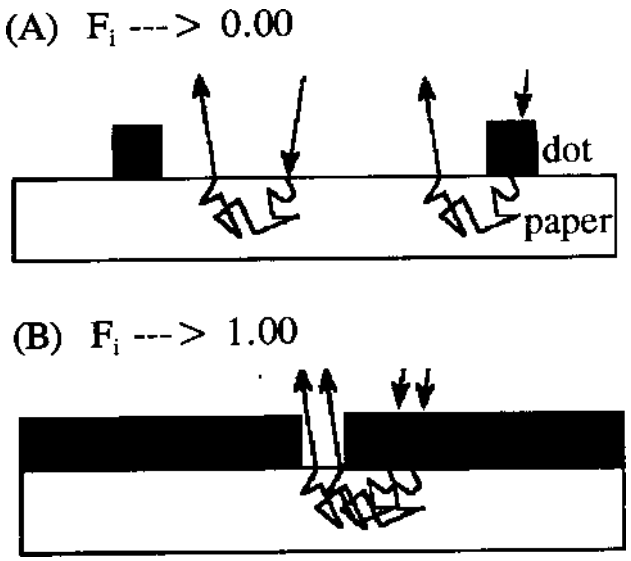

Figure 5. Illustration of the scattering of light relative to the distance between dots. (A) small dots, F_i, near zero, and (B) large dots, F_i near unity.

One can test the efficacy of Eq. 6 as a model for halftone imaging by analysis of histogram data. From the histogram, experimental values of F_i may be determined by integration from $r = 0$ to $r = R_t$. Also, values of $R_i(F_i)$ and $R_p(F_i)$ are measured directly at the histogram peaks. Equation 6 can then be used to calculate the mean image reflectance $R(F_i)$, and this value can be correlated with the reflectance, R_m, measured with a large aperture densitometer or calculated from the overall histogram, using Eq. 3. Figure 6 shows such a correlation for the 65-lpi ink-jet halftone image. For comparison Fig. 7 shows R calculated from the Yule-Nielsen equation correlated with R_m. The value of n in Fig. 7 was chosen to provide the minimum RMS deviation between R_m and $R(F_i)$. It is evident that Eq. 6, essentially the Murray-Davies equation, provides as good a model as the Yule-Nielsen equation, provided that $R_i(F_i)$ and $R_p(F_i)$ are recognized as variable parameters rather than as constants. The experiments shown in Figs. 6 and 7 were repeated for traditional halftone gray scales printed with a variety of printing technologies, and the results are summarized in Table I.

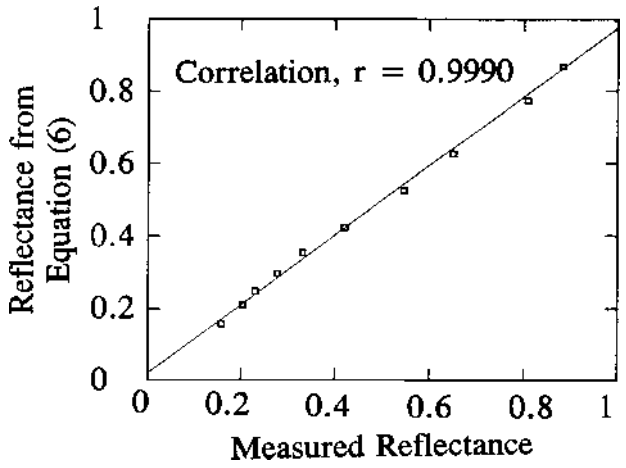

Figure 6. Reflectance values calculated with Eq. 6, using measured values of Ri, Rp, and F versus measured values of macroscopic reflectance.

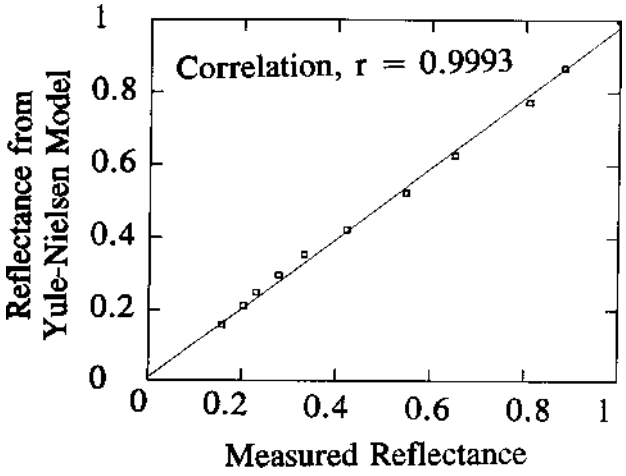

Figure 7. Reflectance values calculated with the Yule-Nielsen equation versus measured values of macroscopic reflectance. The n value was chosen to maximize the correlation coefficient.

Modeling the $R_i(F_i)$ and $R_p(F_i)$ Functions: Light Scattering

The data in Table I indicate that Eq. 6 may indeed serve as a halftone model provided the individual components, $R_i(F_i)$ and $R_p(F_i)$, can be modeled. To develop empirical models of $R_i(F_i)$ and of $R_p(F_i)$, we first examine the behavior of the ink and paper reflectance factors from image histograms as summarized, for example, in Fig. 4. We note that $R_i(F_i)$ and $R_p(F_i)$ vary between limits as F_i varies from 0 to 1. This behavior may be summarized empirically as follows.

$$R_g\, T_i \le R_p(F_i) \le R_g \quad \text{for} \quad 1 \le F_i \le 0$$

and

$$R_g T_i^2 \le R_i(F_i) \le R_g T_i \quad \text{for} \quad 1 \le F_i \le 0$$

Any of a variety of linear and nonlinear functions might be written to model $R_i(F_i)$ and $R_p(F_i)$ between these limits. By trial and error, the following functions have been found to fit experimental data quite well.

$$R_i(F_i) = R_g T_i[1-(1-T_i)F_i^w] \tag{7}$$

$$R_p(F_p) = R_g[1-(1-T_i)(1-F_p^w)], \tag{8}$$

where $F_i = 1 - F_p$.

These functions contain two independently measurable parameters, the bulk reflectance of the unprinted paper, $R_g = R_p$ at $F = 0$, and the transparency of the ink, $T_i = (R_i/R_g)^{1/2}$ for R_i measured at $F_i = 1$. These parameters are analogous to the constants R_i and R_p in the Yule-Nielsen model. Also, as in the Yule-Nielsen model, an arbitrarily chosen power factor, w, is selected to provide the best fit to experimental data. The lines drawn in Figs. 4, 8, and 9 illustrate the fit of Eqs. 7 and 8 to experimental data from three different printing processes. In each case the index of fit was defined as the square root of the mean squared (RMS) deviation between the data points and the model at each value of F_i. The RMS deviation was calculated over both the $R_i(F_i)$ and the $R_p(F_i)$ data for a single index of fit. The same value of w was selected for both the $R_i(F_i)$ and the $R_p(F_i)$ data, and the value of w was selected to minimize the RMS deviation.

TABLE I. Root mean square (RMS) deviation between measured values of reflectance and reflectance calculated with the Murray-Davies equation (Eq. 1), the Yule-Nielsen equation (Eq. 2), and with Eq. 6. Values of Yule-Nielsen *n* were selected to produce the highest correlation.Values of R_i and R_p in Eq. 6 were measured from histogram data at each value of F_i.

		RMS deviation			
Halftone Printing process	frequency, (lpi)	Equation 1 Murray-Davies	Equation 2 Yule-Nielsen	n	Equation 6 New model
Thermal transfer	65	0.063	0.020	1.45	0.016
Ink jet	65	0.045	0.016	1.62	0.019
Ink Jet	100	0.047	0.021	1.70	0.027
Offset litho	65	0.026	0.019	1.60	0.024
Offset litho	150	0.017	0.015	1.40	0.010
1-D offset litho*	60	0.012	0.008	2.0	0.009
Stochastic photo	330dpi†	0.055	0.016	2.0	0.009

* The 1-D system is a one-dimensional halftone with lines instead of dots.

† The stochastic photo process was produced from a film tint contact-printed on was 1800 dpi, and stochastic halftone dots were assembled to be 330 dpi.

An overall model of R versus F_i may then be achieved by combining Eqs. 6, 7, and 8. With only the bulk constants, R_g and T_i, and the power factor, w, a reasonably close fit to the data is achieved, as shown in Figs. 4, 8, and 9.

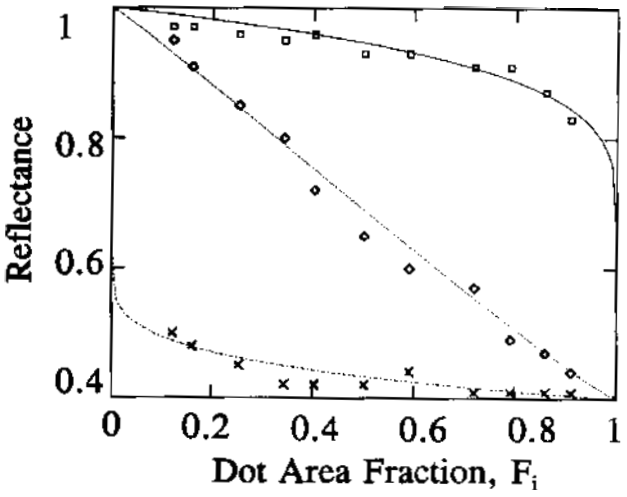

Figure 8. Offset lithographic halftone data at 65 lpi. Reflectance versus dot area fraction, F_i, for overall reflectance $R(F_i)$, ink reflectance $R_i(F_i)$, and reflectance of paper between the dots $R_p(F_i)$. $w = 0.225$.

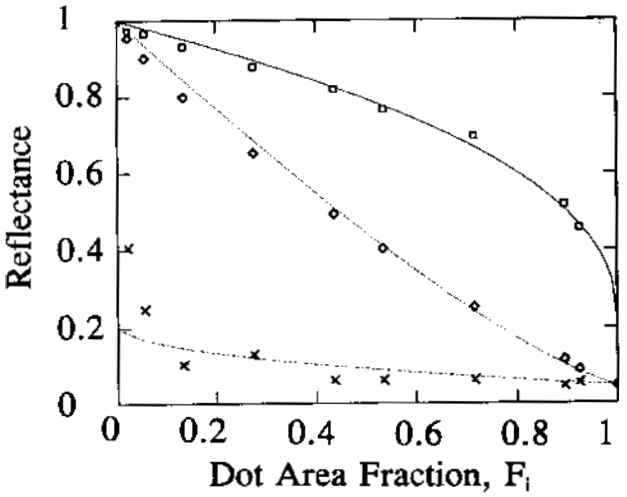

Figure 9. Thermal wax transfer data at 65 lpi. Reflectance versus dot area fraction, Fi, for overall reflectance $R(F_i)$, ink reflectance $R_i(F_i)$, and reflectance of paper between the dots $R_p(F_i)$. $w = 0.443$.

Modeling the $R_i(F_i)$ and $R_p(F_i)$ Functions: Distribution of Transmittancy

The data in Fig. 8 were generated from a 65-lpi halftone gray scale produced with an offset lithographic press. The same press, ink, and paper used to print this 65-lpi gray scale were used to print a 150-lpi halftone gray scale. Histogram analysis of the 150-lpi images resulted in the data shown in Fig. 10. Clearly, the idea that R_i and R_p approach a common limit is not true in this case. The limiting values significantly overshoot each other. Whereas several factors may contribute to this phenomenon, we would like to suggest the following modification to the above empirical model that seems to account for the data quite well.

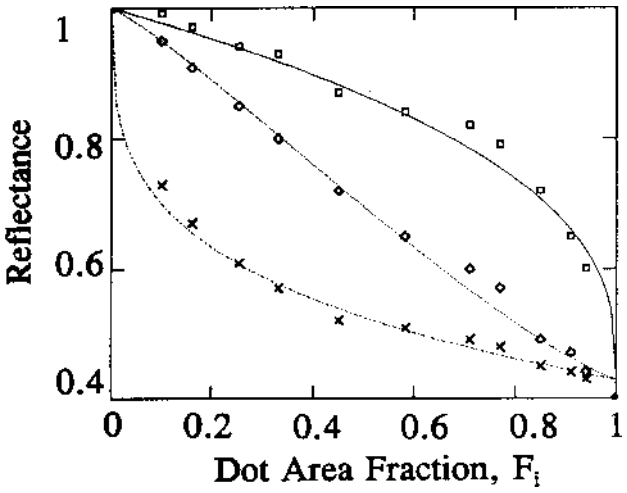

Figure 10. Offset lithographic halftone data at 150 lpi. Reflectance versus dot area fraction, F_i, for overall reflectance $R(F_i)$, ink reflectance, $R_i(F_i)$ and reflectance of paper between the dots, $R_p(F_i)$. $w = 0.357$ and $v = 0.30$.

As suggested schematically in Fig. 11, the edges of dots may not be entirely square. Any feathering of the dot near its edge will result in a dot transmittance, T_i, that is lower near the edge of the dot. If this occurs, then the transmittance, T_i, in Eq. 7 will approach zero as F_i approaches zero. To account for this behavior, we would like to suggest substituting for the product R_gT_i in Eq. 7 a function that varies from R_gT_i to R_g as F_i varies from 1 to 0. The following model is proposed

$$R_i(F_i) = R_g[1-(1-T_i)F_i^w]\cdot[1-(1-T_i)F_i^v]. \qquad (9)$$

Similarly, as F_i approaches unity, the paper between the dots may fill with colorant, as suggested schematically in Fig. 11. If this occurs, then the apparent reflectance of the paper will decrease. To account for this behavior, we would like to suggest substituting for R_g in Eq. 8 a function that varies from R_g to R_gT_i as F_i varies from 0 to 1, or as F_p varies from 1 to 0. The following model is proposed.

$$R_p(F_p) = R_g[1-(1-T_i)(1-F_p^w)]\cdot[1-(1-T_i)F_p^v] \qquad (10)$$

The power factor, v, may be thought of as a factor that models the softness of the dot edges. If $v = 0$, the dots are perfectly sharp and Eqs. 9 and 10 reduce to Eqs. 7 and 8. However, with addition of this dot softness function to the model, the *solid lines* shown in Fig. 10 result and provide a reasonable fit to the data. Similarly, the data shown for the thermal print engine at 65 lpi and the stochastic image at 330 lpi are shown in Figs. 12 and 13. The values of $R_i(F_i)$ and $R_p(F_i)$ in these cases also can be fit well with the proposed model only with $v > 0$.

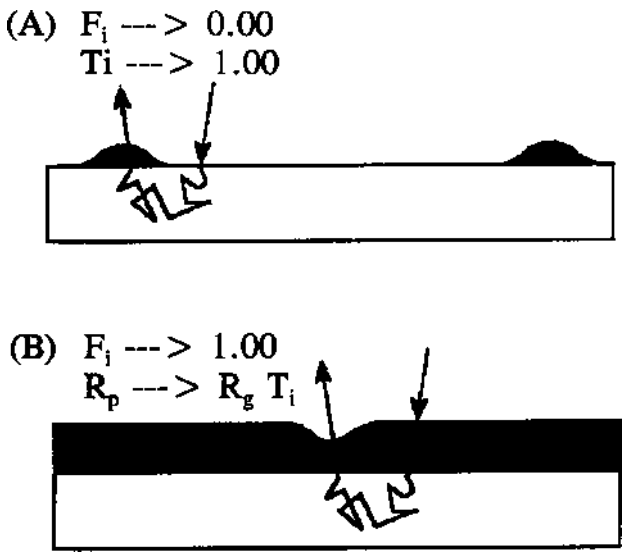

Figure 11. Illustration of the scattering of light relative to thedistance between dots and the shape of the dot edges. (A) small dots F_i near zero, and (B) large dots, F_i near unity.

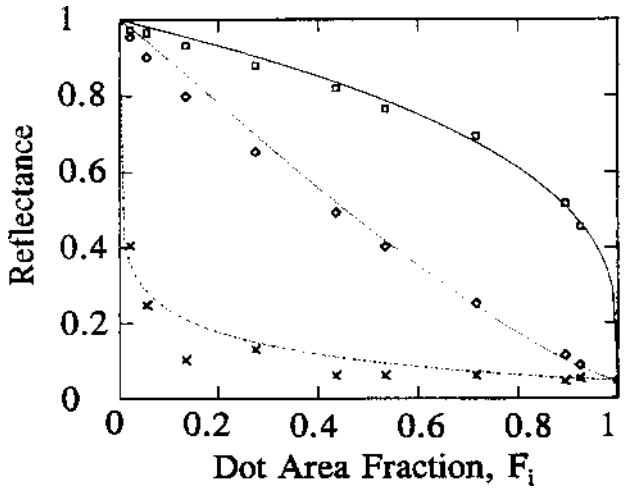

Figure 12. Thermal wax transfer data at 65 lpi. Reflectance versus dot area fraction, F_i for overall reflectance $R(F_i)$, ink reflectance $R_i(F_i)$, and reflectance of paper between the dots $R_p(F_i)$. $w = 0.31$ and $v = 0.10$.

Discussion

The values of n chosen to fit the Yule-Nielsen equation typically lie between 1 and 2. Pearson,[13] for example, suggests a mean value of 1.7 to fit most routine applications of the Yule-Nielsen function. Moreover, theoretical analysis suggests that $n = 2$ is a theoretical limit unless factors other than the optical scattering of light are involved.[11] Both w and v in the model suggested by Eqs. 6, 9, and 10 are limited to the range 0 to 1 by the empirical arguments from which the equations were derived. If one compares the behavior of the Yule-Nielsen equation with Eqs. 6, 9, and 10, it is easy to demonstrate that the two models are numerically identical under some, but not all, conditions. For example, both models reduce to Murray-Davies at $n = 1$ and at $w = v = 0$. Moreover, the new model produces numerically identical results to Yule-Nielsen at $n = 2$ when either w or v is unit. However, at intermediate values of n, w, and v, the two models do not produce identical numerical results at every value of F_i. It may be possible, therefore, to observe a better fit of one model over another, provided experimental error can be reduced sufficiently to detect the difference between the models. Thus far, the experimental variability in the data we have generated is insufficient to distinguish the two models.

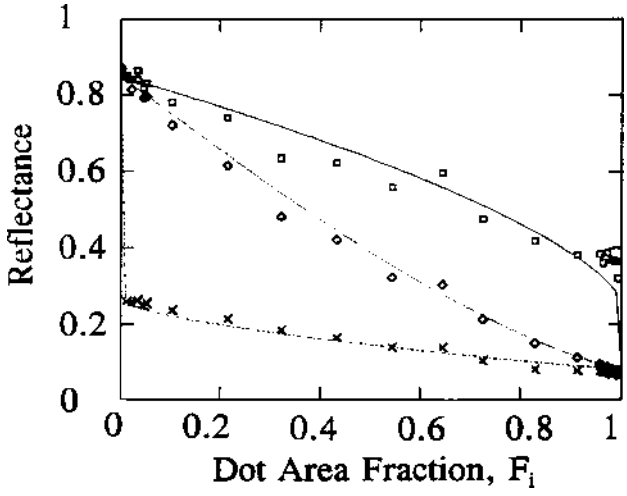

Figure 13. Stochastic halftone at 330 lpi. Reflectance versus dot area fraction, F_i, for overall reflectance $R(F_i)$, ink reflectance, $R_i(F_i)$, and reflectance of paper between the dots, $R_p(F_i)$. $w = 0.654$ and $v = 0.003$.

The new model, with constants w and v, has a disadvantage over the Yule-Nielsen model in that it is more complex to apply and does not provide a clear advantage to fitting R versus F_i data. The new model does, however, provide a description of some features of the image microstructure. That is, $R_i(F_i)$ and $R_p(F_i)$ are also modeled. Moreover, two different effects, the light-scattering effect and the dot-shape effect, are separately modeled. Unfortunately, the functions that model dot-shape and scattering are identical, and this leads to some ambiguity. Based solely on R, R_i, and R_p data versus F_i, one cannot unambiguously distinguish between scattering and dot-shape effects. While the model can be compared directly with experimentally observed values of $R_i(F_i)$ and $R_p(F_i)$, measured dot profiles of T_i, or of mean dot T_i versus F_i have not been achieved experimentally. Such additional image microstructure information would be of considerable interest in further developing the model. Nevertheless, the current model does preserve the linearity of photon additivity and is offered as an incremental advance in both our experimental and theoretical understanding of the optical properties of ink-on-paper images.

Acknowledgments

The authors would like to express their appreciation to the 3M Company for support of this project. Special

thanks to Richard Fisch for encouragement and guidance in the directions and priorities of the project. Thanks also to Bruce Blom of Mead Central Research for encouragement and advice.

Appendix A: Experimental Procedures

Image Capture and Reflectance Calibration

The images in this study were captured with a Model 4810 CCD camera (COHU Electronics, San Diego, CA) onto a VISONplus-AT OFG frame grabber (Imaging Tech. Inc., Bedford, MA) in a 486/50/DX2 type PC. The frame grabber and camera were controlled by IMLAB software (Warner Frei, Santa Monica, CA). The image field of view was 2.50 × 2.26 mm, and the image was digitized at a pixel resolution of 512 × 462. Image analysis was accomplished with software routines developed by the authors, and the IMLAB software provided an available and convenient shell for writing and running the programs. Illumination was achieved with a ring fiber optic illuminator attached to the microscope objective. As shown previously,[14] the pixel values from the camera used in this work are linear with respect to the reflectance factor of the object being imaged. Pixel values were translated into reflectance factors by calibration against a dark frame, captured with the lens cap in place, and against a white reference. In all cases, the white reference was an unprinted region of the paper itself. Thus reflectance values reported in this project are all relative to the reflectance of the paper substrate. Except for the stochastic gray scales, the same paper was used for all experiments. The paper was a coated sheet with a measured visual reflectance of 0.87.

Calculation of Fractional Dot Area, F_i

Once the image had been captured and calibrated, it was displayed on a relative pixel scale of 0 to 255, corresponding to a reflectance range of 0 to 1. An image histogram, defined as the frequency distribution of reflectance values in the image, was calculated. Figure 2 is an illustration. The reflectance value in the histogram corresponding to the transition point between dot and paper was defined as the region of maximum rate of change in pixel value, dR/dx, in moving from the center of a dot (R_{min}) to the center of the paper (R_{max}). This transition reflectance, called R_t in Eq. 4, was estimated experimentally by performing a software line scan across the images of several dots and numerically averaging several transition reflectances. The value of F_i was then determined by integrating the image histogram up to the mean value of R_t.

Halftone Samples

With the exception of the stochastic gray scale, all halftones were printed on the same coated paper stock. Offset lithographic images were printed by the RIT T&E Center, using oil-based ink. Thermal-transfer and ink-jet images were printed by the RIT Research Corporation on proprietary laboratory machines. The thermal transfer engine was a CalComp 6603-XF, capable of 300-dpi resolution, with a thermal wax transfer ribbon. The ink jet was a Canon BJC-600, bubble-jet engine capable of 360-dpi resolution, The stochastic, or "FM" halftone gray scale was a UGRA Select Velvet screen generated with an Agfa Select Set 7000 image setter. The output screen tint was contact printed onto Kodak Quartz Contact Paper, a very high resolution, high-contrast photographic print paper.

Appendix B: Glossary

F_i = Dot area fraction.
F_p = Paper area fraction, $F_p = 1 - F_i$.
R_i = Reflectance of the halftone ink dot, assumed to be a constant in Eqs. 1 and 2,
R_p = Reflectance of the paper between the dots, assumed to be a constant in Eqs. 1 and 2.
R_g = Intrinsic reflectance of the paper substrate at $F_i = 0$,
T_i = Intrinsic transmittance of the ink layer of the dot at $F_i = 1$,
$R_p(F_p)$ = Mean value of reflectance of paper between halftone dots, measured experimentally from a peak in the histogram distribution of reflectance, and observed to be a function of the dot area fraction, F_i.
$R_i(F_i)$ = Mean value of halftone ink dot, measured experimentally from a peak in the histogram distribution of reflectance, and observed to be a function of the dot area fraction, F_i.
$H(R)$ = Relative frequency of occurrence of a given R in a histogram.
R_t = Reflectance at the boundary between ink dot and paper, used to signify the threshold between ink and paper,

References

1. A. Murray, *J. Franklin Inst*. **221**: 721 (1936).
2. H. E. J. Neugebauer, *Tech. Phys*. **38**: 75 (1937).
3. J. A. Yule and W. J. Nielsen, *TAGA Proceedings*, 1951, p. 65.
4. J. A. S. Viggiano, *TAGA Proceedings*, 1985, p. 647.
5. J. S. Harrington, *TAGA Proceedings*, 1991, p. 144.
6. Y. Shiraiwa and T. Mizuno, *J. Imaging Sci. Technol*., **37**: 385 (1993).
7. W. W. Pope, *TAGA Proceedings*, 1989, p. 142.
8. F. R. Clapper and J. A. Yule, *J. Opt Soc. Am*. **43**: 600 (1953).
9. F. P. Callahan, *J. Opt Soc. Amer*. **42**:104, (1952).
10. J. A. C. Yule, O. J. Howe, and J. H. Altman, *TAPPI* **50**: 337 (1967).
11. F. Ruckdeschel and O. G. Hauser, *Appl. Opt.* **17**: 3376 (1978).
12. J. R. Huntsman, *J. Imaging Technol.* **13**: 136 (1987).
13. M. Pearson, *TAGA Proceedings*, 1980, p. 415.
14. J. S. Arney and D. Stewart, *J. Imaging Sci. Technol*. **37**: 504 (1993).

❋ Previously published in the *Journal of Imaging Science and Technology*, 39(6) pp. 502–508, 1995.